Berenguer Betrián, R.; Sieben, JM.; Quijada Tomás, C.; Morallón, E. (2016). Electrocatalytic degradation of phenol on Pt- and Ru-doped Ti-SnO2-Sb anodes in an alkaline medium. Applied Catalysis B: Environmental. 199:394-404. doi:10.1016/j.apcatb.2016.06.038.

Electronic Supplementary Information

Electrocatalytic degradation of phenol on Pt- and Ru-doped Ti/SnO_2-Sb anodes in an alkaline medium

R. Berenguer[a], J.M. Sieben[b], C. Quijada[c], E. Morallón[a,*]

[a] Departamento de Química Física and Instituto Universitario de Materiales, Universidad de Alicante, Apartado 99, E-03080 Alicante, Spain.

[b] Instituto de Ingeniería Electroquímica y Corrosión and CONICET, Universidad Nacional del Sur, Av. Alem 1253, (B8000CPB) Bahía Blanca, Argentina.

[c] Departamento de Ingeniería Textil y Papelera, Universidat Politècnica de València, Plaza de Ferrándiz y Carbonell, E-03801 Alcoy (Alicante), Spain.

* Corresponding author: morallon@ua.es

Appendices

The basis for our generalized kinetic model is the same than that of the model developed earlier by Comninellis et al. [1,2] for ideal non-active electrodes, such as BDD electrodes. A simplified reaction scheme is considered in which electrogenerated adsorbed hydroxyl radicals are intermediate species involved in both the target reaction of oxidation of organics and the side reaction of oxygen evolution on a non-active metal oxide anode:

$$MO_x + H_2O \rightarrow MO_x(OH^{\bullet})_{ads} + H^+ + e$$

$$MO_x(OH^{\bullet})_{ads} + Organics \rightarrow MO_x + Mineralization\ Prods + H^+ + e$$

$$MO_x(OH^{\bullet})_{ads} \rightarrow MO_x + \frac{1}{2}O_2 + H^+ + e$$

The model relies on the following assumptions: i) the adsorption of the organic compound at the electrode surface is negligible, ii) the oxidation of organics is a fast reaction controlled by mass transport to the anode surface and iii) bulk oxidation with electrogenerated oxidants (like H_2O_2, O_3, etc) is not considered. Depending on the applied current density, j_{app}, two kinetic regimes can be distinguished under galvanostatic electrolysis operation in recirculating batch electrochemical reactors: i) when j_{app} is lower than the limiting current density, j_{lim}, the electrolysis is under current control; organic matter is thereby removed at the same (constant) rate than electrons are supplied from the external power source. As COD is lowered during the course of electrolysis, j_{lim} decreases accordingly to equal j_{app} at a certain transition time (or transition COD conversion); ii) when$j_{app} > j_{lim}$ (beyond the transition time): the rate is limited by mass transport, and the concentration of organic matter decreases exponentially with the increasing electrolysis time. Thus, this model predicts the occurrence of a region showing pseudo zero-order kinetics with constant rate independent of organics concentration, a linear decay of COD with time and 100 % current efficiency (all applied current is employed in the removal or organics) and the occurrence of a region showing pseudo first-order kinetics, with an exponential decay of COD with time and current efficiency below 100% because of part of the current is wasted in side reactions like OER. For a more detailed description of this predictive model the reader is referred to excellent reviews in refs [1,2].

In our generalized model, a convenient modification is introduced in order to recognize nonidealities arising from the possibility that adsorbed hydroxyl radicals may undergo fast

oxidative recombination to yield evolving oxygen even when the oxidation of organics proceeds under current control. In other words, the OER is treated as a competing reaction under all electrolysis conditions.

Additional approximations to be borne in mind for galvanostatic electrolysis of organic matter solutions in recirculated batch mode are: i) the electrolyte is perfectly mixed in both the electrochemical cell and the auxiliary reservoir and ii) the volume of the reservoir is much larger than that of the electrochemical reactor. Then, appropriate kinetic equations can be derived from mass balances over the electrochemical reactor and reservoir to describe the time evolution of either a single organic species like phenol (Appendix A) or COD (Appendix B) in the batch recirculation electrolytic system.

Appendix A. Kinetic model for phenol oxidation

The heterogeneous rate of phenol oxidation (r) is expressed as:

$$r = \frac{j_{Ph}}{nF} \text{ (in mol m}^{-2}\text{s}^{-1}\text{)} \quad \text{(A 1)}$$

Where j_{Ph} is the current density (A m^{-2}) effectively employed in the electrochemical conversion of phenol, with an exchange of n (unknown) electrons, and F is the Faraday constant (96485 C mol^{-1}).

The electrolysis can be run under two kinetic regimes, depending on the relative values of the applied current density, j_{app}, or more precisely, j_{Ph}, and the limiting current density (j_{lim}; A m^{-2}) for the oxidation of phenol ($j_{lim} = nFk_m[Ph]$), where k_m is the mass transfer coefficient (in m s^{-1}) and [Ph] is the phenol concentration (mol m^{-3}).

(a) Zone I. Electrolysis is under current control and kinetics is of the pseudo zero-order.

This kinetic regime is observed whenever $j_{Ph} < j_{lim}$ and the mass transfer rate is fast enough to replenish the electrode surface with new reactant molecules.

The effective current density for phenol oxidation, j_{Ph}, is related to the applied current density, j_{app} according to:

$$j_{Ph} = CE_0 j_{app} \quad \text{(A 2)}$$

Where CE_0 is the initial or zero-order current efficiency for phenol oxidation. Within this region phenol is being oxidized at a constant rate independently of its concentration and hence CE_0 is kept constant. It can be then considered as a factor measuring the deviation from the ideal behavior, i.e, ideal non-active anodes should exhibit CE_0 close to 100 % while working under this regime.

Combining mass-balance equations over the electrochemical reactor and the reservoir we obtain:

$$\frac{d[Ph]}{dt} = -\frac{CE_0}{n}\frac{j_{app}A}{FV} \quad \text{(A 3)}$$

Where A is the area of electrode (m^2), and V the volume of the electrolyte (m^3). The integration of this differential equation with the initial condition [Ph] = $[Ph]_0$ at t=0 yields the following time-dependent expression for the normalized phenol concentration:

$$\frac{[Ph]}{[Ph]_0} = 1 - \frac{CE_0}{n}\frac{j_{app}A}{FV[Ph]_0}t \quad \text{(A 4)}$$

All the electrolysis constants can be grouped in an apparent zero-order rate constant, k_0 (mol m^{-3} s^{-1}):

$$k_0 = \frac{CE_0}{n}\frac{j_{app}A}{FV} \quad \text{(A 5)}$$

The phenol concentration decreases linearly with the electrolysis time and so does the limiting current density. The above behavior persists until a given phenol conversion is achieved at a certain transition or critical time at which $CE_0 j_{app} = j_{lim}$ (t_c). At this point we introduce the dimensionless parameter, β:

$$\beta = CE_0\frac{j_{app}}{j_{lim}^0} \quad \text{(A 6)}$$

Where j_{lim}^0 is the initial limiting current density, given by:

$$j_{lim}^0 = nFk_m[Ph]_0 \quad \text{(A 7)}$$

Note that Eq.(A 6) can be rewritten as:

$$\beta = CE_0\alpha \quad \text{(A 8)}$$

With α having a similar meaning than the characteristic parameter defined by Comninellis et al. [1,2].

The application of the critical condition at time t_c leads to:

$$\beta j_{lim}^{0} = j_{lim}(t_c) = nFk_m[Ph]_c$$

$$[Ph]_c = \beta[Ph]_0 \quad \text{(A 9)}$$

The critical time can be calculated by substituting Eq. (A 9) in (A 4):

$$t_c = \frac{1-\beta}{\beta}\frac{V}{k_m A} \quad \text{(A 10)}$$

(b) Zone *II*. Electrolysis is a mass-transport limited process and kinetics is of the pseudo first-order.

Beyond the transition time or whenever $j_{Ph}=j_{lim}$, the heterogeneous phenol oxidation rate is of pseudo first-order with respect to phenol concentration:

$$r = \frac{j_{lim}}{nF} = k_m[Ph] \quad \text{(A 11)}$$

In this case mass balances on the electrochemical reactor and the reservoir give rise to:

$$\frac{d[Ph]}{dt} = -\frac{k_m A}{V}[Ph] \quad \text{(A 12)}$$

The integration of Eq. (A 12) from $t=t_c$ to t and $[Ph]=[Ph]_c$ to $[Ph](t)$ results in:

$$\frac{[Ph]}{[Ph]_0} = \beta \exp\left(-\frac{k_m A}{V}t + \frac{1-\beta}{\beta}\right) \quad \text{(A 13)}$$

A pseudo-first order rate constant, k_1 (s^{-1}), directly related to the mass transfer coefficient, can be then defined:

$$k_1 = \frac{k_m A}{V} \quad \text{(A 14)}$$

Within this region, the current efficiency is no longer constant. The instantaneous current efficiency, *ICE*, is defined as:

$$ICE = \frac{j_{lim}(t)}{j_{app}} = \frac{[Ph]}{\alpha[Ph]_0} = \frac{CE_0}{\beta}\frac{[Ph]}{[Ph]_0}$$

$$ICE = CE_0 \exp\left(-k_1 t + \frac{1-\beta}{\beta}\right) \quad \text{(A 15)}$$

Since the number of electrons involved in the electrochemical transformation of phenol is unknown, this relation can be more conveniently expressed in terms of the *ICE*/n ratio:

$$\frac{ICE}{n} = \frac{CE_0}{n} \exp\left(-k_1 t + \frac{1-\beta}{\beta}\right) \quad \text{(A 16)}$$

Appendix B. Kinetic model for COD removal

The analysis of COD removal provides a better understanding and measure of the non-selective decontamination process at metal oxide anodes, as well as a more precise evaluation of its efficiency. In this case, the heterogeneous rate constant is:

$$r = \frac{j_{COD}}{4F} \quad \text{(B 1)}$$

where j_{COD} refers to the current density used up to the complete mineralization of organic matter involved in the electrolysis of phenol. Again, two different operating regimes can be discerned depending on the relative values of j_{COD} and the limiting current density for COD removal ($j_{lim}^{COD} = 4Fk_m COD$):

(a) Zone I. Electrolysis is under current control ($j_{COD} < j_{lim}^{COD}$).

By analogy to the description made in Appendix A, j_{COD} can be expressed as a function of the applied current density and the initial current efficiency for COD removal, CE'_0, which remains constant within this kinetic regime and it departs from 100 % as long as the behavior of the anode deviates from that expected for an ideal non-active electrode:

$$j_{COD} = CE'_0 j_{app} \quad \text{(B 2)}$$

A similar mathematical treatment to that described in Appendix A leads to a linear dependence of the normalized COD change with the increasing time:

$$\frac{COD}{COD_0} = 1 - CE'_0 \frac{j_{app} A}{4FVCOD_0} t \quad \text{(B 3)}$$

And an apparent zero-order rate constant for COD removal, k'_0, (mol $m^{-3}s^{-1}$) can be defined as:

$$k_0' = CE_0' \frac{j_{app} A}{4FV} \quad \text{(B 4)}$$

At the critical or transition time:

$$CE_0' j_{app} = j_{lim}^{COD}(t_c) \quad \text{(B 5)}$$

And:

$$COD_c = \beta' COD_0 \quad \text{(B 6)}$$

Where:

$$\beta' = CE_0' \alpha' \quad \text{(B 7)}$$

$$\alpha' = \frac{j_{app}}{j_{lim}^{COD,0}} \quad \text{(B 8)}$$

$$j_{lim}^{COD,0} = 4Fk_m COD_0 \quad \text{(B 9)}$$

By following the same procedure as in Appendix A, an expression for the critical time is:

$$t_c = \frac{1-\beta'}{\beta'} \frac{V}{k_m A} \quad \text{(B 10)}$$

(b) Zone *II*. Electrolysis is mass-transport limited ($j_{COD}=j_{lim}^{COD}$)

Now, the rate for COD removal is of first order with respect to COD:

$$r = \frac{j_{lim}^{COD}}{4F} = k_m COD \quad \text{(B 11)}$$

The solution of mass-balance system of differential equations from $t=t_c$ to t and $COD=COD_c$ to COD (t) gives the temporal evolution of the COD:

$$\frac{COD}{COD_0} = \beta' exp\left(-\frac{k_m A}{V} t + \frac{1-\beta'}{\beta'}\right) \quad \text{(B 12)}$$

An apparent pseudo first-order rate constant, k'_1 (s^{-1}) can be also defined that is related to the mass transport coefficient in an analogous way than k_1.

Finally the instantaneous current efficiency for COD removal, *ICE'*, is expected to change with time according to:

$$ICE' = CE'_0 \exp\left(-k'_1 t + \frac{1-\beta'}{\beta'}\right) \quad \text{(B 13)}$$

Formation of fouling films during electrolysis

Small yellowish-brown fragments with lamellar shape were observed in the electrolyte solution and/or as solid residue on the electrodes during the electrolytic treatments of phenolate solutions in this work. The formation of these products generally occurred on the surface of the different studied electrodes, and mainly in the case of Ti/RuO_2.

The presence of similar substances was previously detected also by others authors upon the electrolysis of phenolic wastewaters, being assigned to a mixture of various polymeric compounds of low molecular weight [3,4]. In other to confirm this, the nature and structure of the solid residue formed on the electrodes was investigated by transmission electron microscopy (JEOL JEM-2010), which was coupled to an Oxford X-ray detector for energy dispersive X-ray (EDX) microanalysis.

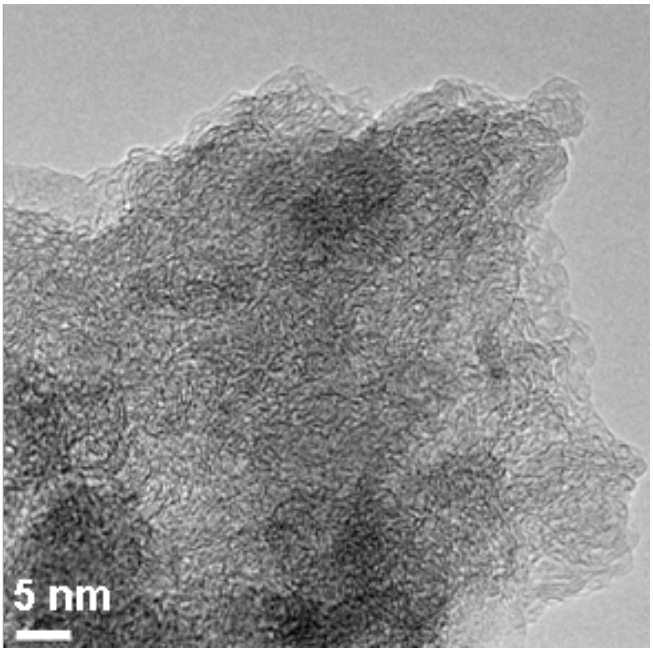

Figure S1. TEM image of a solid fragment found on the surface of the Ti/RuO_2 mesh electrode after the electrolysis of 1000 ppm Ph/0.5 M NaOH solution at 10 mA cm^{-2}.

Figure S1 shows the TEM image of one of the small fragments collected from the surface of the Ti/RuO_2 electrode. As it can be observed, these fragments are composed of disordered

domains with an amorphous-like structure. On the other hand, EDX revealed that the major component of the sample is carbon (93 at. %). These results seem to confirm the formation of polymeric chains retained on the electrode surface.

According to Li et al., the high electroactivity of RuO_2 anodes for OER could shorten the lifetime of quimisorbed hydroxyl radicals, what may hamper the oxygen transfer from the radicals to the organics for their electro-oxidation [5]. Therefore, the aromatic ring opening takes place slowly and polymerization becomes more significant in this kind of active oxides, in agreement with the obtained results.

Additional galvanostatic experiments in a phenolate-free alkaline electrolyte revealed that the studied applied currents and/or the formation of oxygen bubbles (OER) were able to detach these blocking polymers from the electrode surface. Hence, as pointed in the main text, the kinetics of the electroxidation of phenolic alkaline wastewaters on metal oxides could be highly affected or dominated by the continuous formation and detachment of blocking polymers.

Quantification of benzoquinone during the electrolysis of alkaline phenolic wastewater

The concentration of benzoquinone was determined by UV-Vis spectroscopy. As it can be observed in Figure S2a, the wavelength of the maximum absorbance of p-benzoquinone (BQ) pattern at 319 nm coincides with that of the new band identified in the electrolyte solution during the electrolysis of phenol solutions (see Fig. 4a of the main text). Moreover, the figure also shows that this maximum can be easily distinguished from that of phenolate (at 269 nm), although both bands seem to overlap in some extent.

In order to study the interference of both bands, several mixes of phenol and BQ with different proportions were analyzed by this technique (Figures S2b and S2c). The observed change on the absorbance at 269 nm with an increasing proportion of BQ (Fig. 2Sb) clearly indicates that the presence of BQ affects the maximum absorbance of phenolate band, thus, preventing its quantification from these spectra. However, the maximum absorbance of BQ at 319 nm seems to be practically unaffected by the presence of phenolate in different proportions (Fig. S2c). Hence, the concentration of BQ can be estimated from the absorbance at 319 nm. Nevertheless, the presence of other quinones, like o-BQ, should not be ruled out.

Fig. S2d shows, as example, the spectra of various patterns of BQ prepared to obtain the calibration curve at 319 nm (Fig. S2e). For the calculation of BQ concentration in the electrolyte during the electrolysis of phenol, samples of 20 µL were diluted into the range of 0-50 ppm.

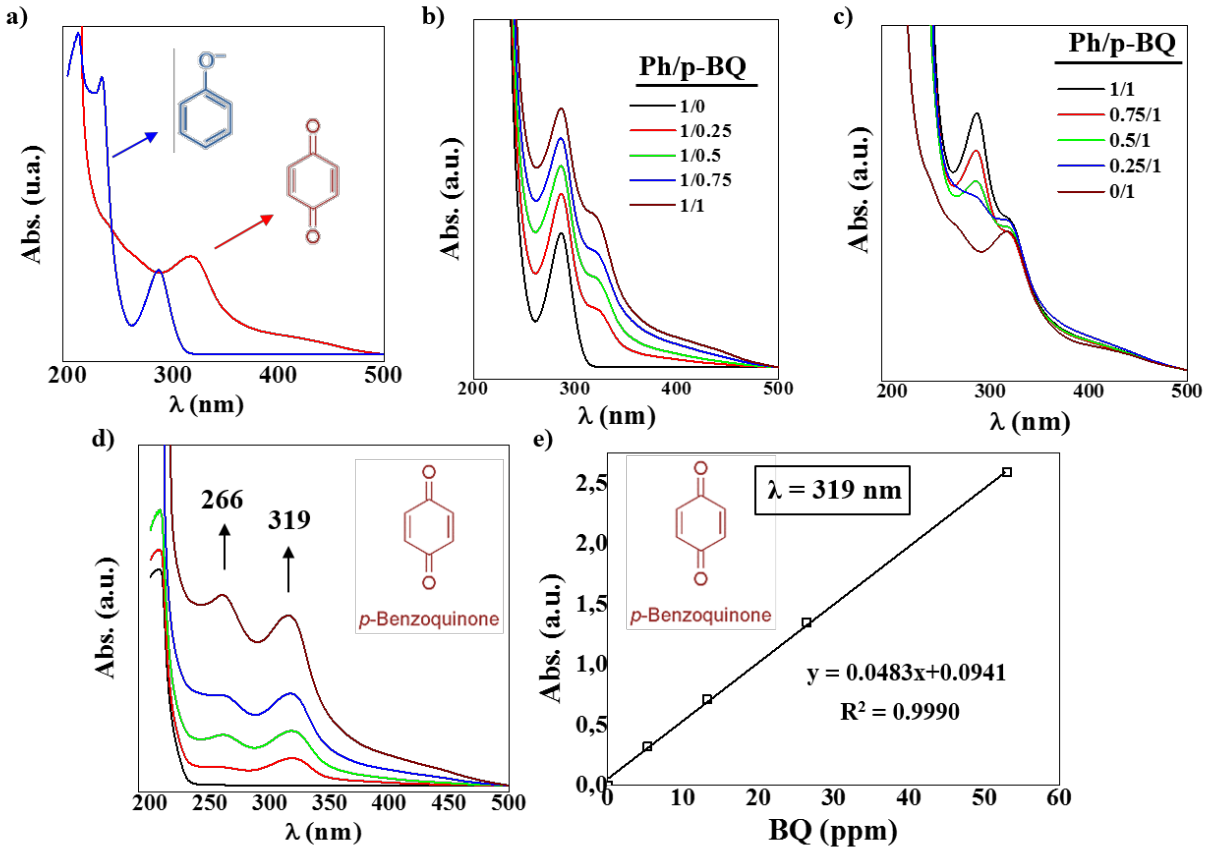

Figure S2. UV spectra of (a) phenol and p-benzoquinone patterns; (b,c) binary mixes of phenol and p-benzoquinone patterns with different ratios; and (d) p-benzoquinone patterns of different concentrations, in 0.5 M NaOH solution; (e) calibration curve of p-benzoquinone at 319 nm (from (d)).

Phenol and COD decays expressed in terms of specific charge passed

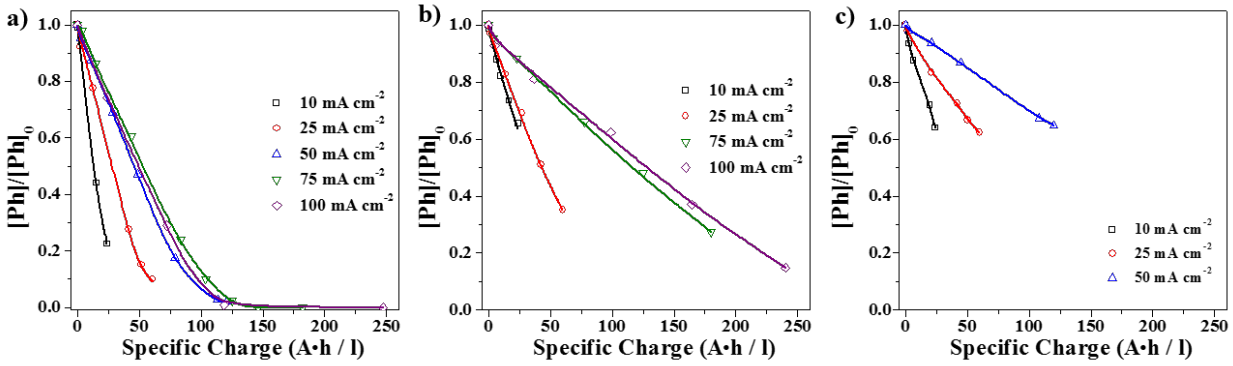

Figure S3. Evolution of the normalized phenolate concentration with charge passed for (a) Ti/SnO_2-Sb-Pt; (b) Ti/SnO_2-Sb(9.75)-Pt-Ru(3.25); (c) Ti/SnO_2-Sb(3.25)-Pt-Ru(9.75) at different current densities (electrolyte = 1000 ppm Ph/0.5 M NaOH).

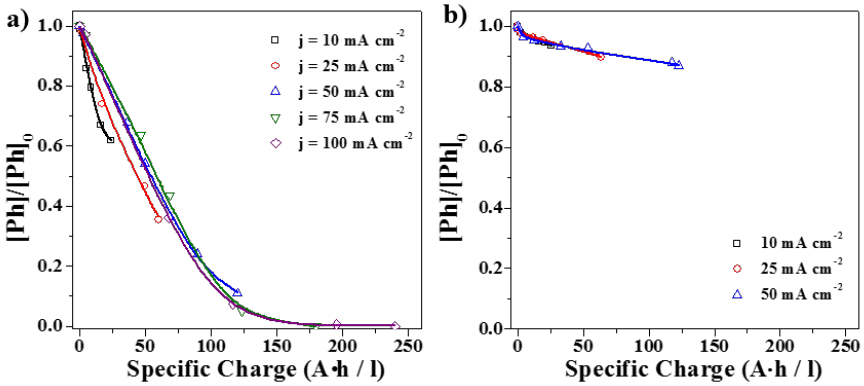

Figure S4. Evolution of the normalized phenolate concentration with charge passed for (a) Ti/RuO_2 and (b) Ti/Co_3O_4 anodes at different current densities (electrolyte = 1000 ppm Ph/0.5 M NaOH).

The relevant kinetic equations expressed as a function fo the specific charge and the ensuing kinetic rate constants are:

Zone I: $\frac{[Ph]}{[Ph]_0} = 1 - \frac{k_0''}{[Ph]_0} Q_{sp}$; $\quad k_0'' = \frac{3600 CE_0}{nF}$ $\quad$ mol A^{-1} h^{-1}

Zone II: $\frac{[Ph]}{[Ph]_0} = \beta \exp\left(-k_1'' Q_{sp} + \frac{1-\beta}{\beta}\right)$; $\quad k_1'' = \frac{k_m A}{I_{app}}$; $\quad$ L A^{-1} h^{-1}

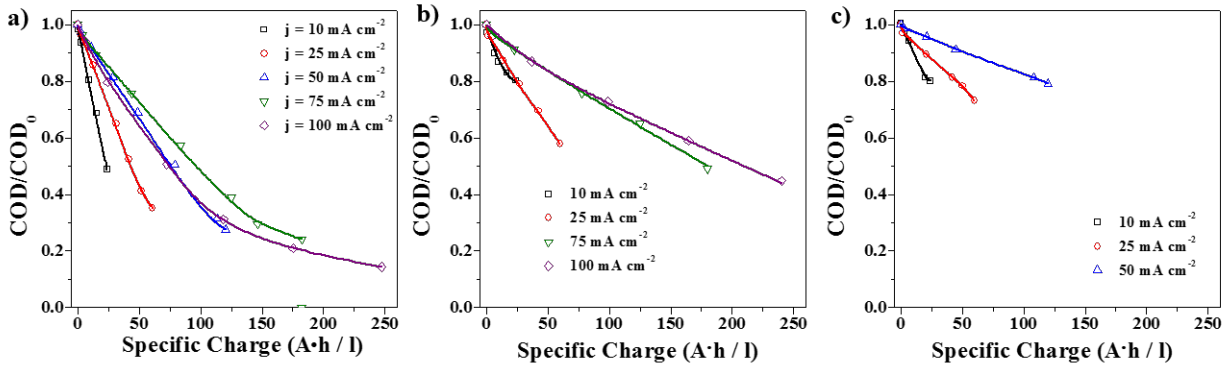

Figure S5. Evolution of the normalized COD with charge passed for (a) Ti/SnO_2-Sb-Pt; (b) Ti/SnO_2-Sb(9.75)-Pt-Ru(3.25); (c) Ti/SnO_2-Sb(3.25)-Pt-Ru(9.75) at different current densities (electrolyte = 1000 ppm Ph/0.5 M NaOH).

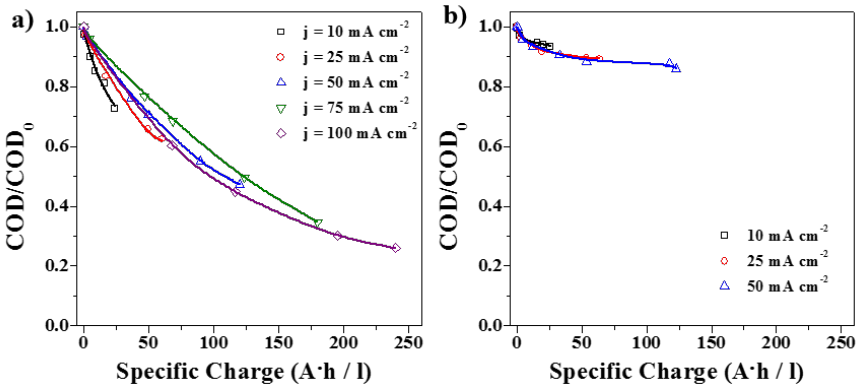

Figure S6. Evolution of the normalized COD with charge passed for (a) Ti/RuO_2 and (b) Ti/Co_3O_4 anodes at different current densities (electrolyte = 1000 ppm Ph/0.5 M NaOH).

The relevant kinetic equations expressed as a function fo the specific charge and the ensuing kinetic rate constants are:

Zone I: $\frac{COD}{COD_0} = 1 - \frac{k_0'''}{COD_0} Q_{sp}$; $\quad k_0''' = \frac{3600 CE_0'}{4F}$ $\quad$ mol A^{-1} h^{-1}

Zone II: $\frac{COD}{COD_0} = \beta \exp\left(-k_1''' Q_{sp} + \frac{1-\beta}{\beta}\right)$; $\quad k_1''' = \frac{k_m A}{I_{app}}$; $\quad$ L A^{-1} h^{-1}

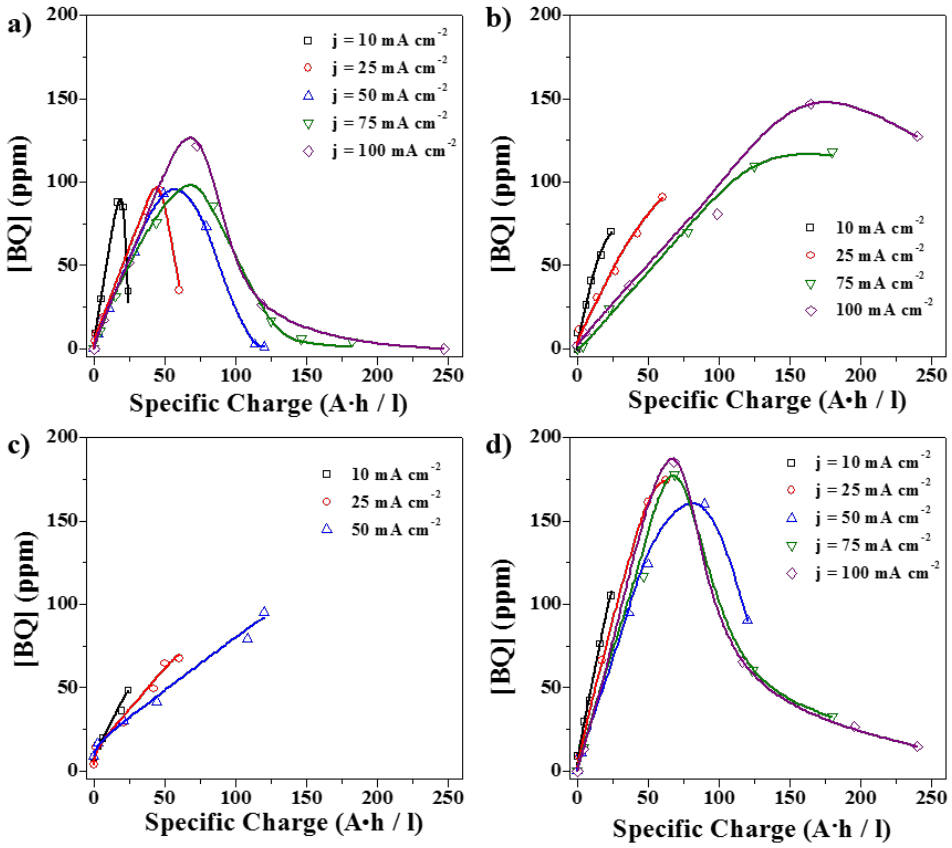

Figure S7. Evolution of benzoquinone concentration with charge passed during the electrochemical treatment of 1000 ppm Ph/0.5 M NaOH solution at different current densities using (a) Ti/SnO_2-Sb-Pt; (b) Ti/SnO_2-Sb(9.75)-Pt-Ru(3.25); (c); Ti/SnO_2-Sb(3.25)-Pt-Ru(9.75); and (d) Ti/RuO_2.

References

[1] M.A. Rodrigo, P.A. Michaud, I. Duo, M. Panizza, G. Cerisola, Ch. Comninellis, J. Electrochem. Soc. 148 (2001) D60-D64.

[2] M. Panizza, P.A. Michaud, G. Cerisola, Ch. Comninellis, J. Electroanal. Chem., 507 (2001) 206-214.

[3]. Ch. Comninellis, C. Pulgarin, J.Appl. Electrochem. 21 (1991) 703-708.

[4]. P. Cañizares, F. Martínez, J. García-Gómez, C. Sáez, M.A. Rodrigo, J. Appl. Electrochem. 32 (2002) 1241-1246.

[5]. X.Y Li, Y.H. Cui, Y.J. Feng, Z.M. Xie, J.D. Gu, Water Res. 39 (2005) 1972-1981.